

Direct Measurement of Transition Frequencies in Isolated $\bar{p}\text{He}^+$ Atoms, and New CPT -Violation Limits on the Antiproton Charge and Mass

M. Hori,¹ J. Eades,² R. S. Hayano,² T. Ishikawa,² W. Pirkel,² E. Widmann,² H. Yamaguchi,² H. A. Torii,³ B. Juhász,⁴ D. Horváth,⁵ and T. Yamazaki⁶

¹CERN, CH-1211 Geneva 23, Switzerland

²Department of Physics, University of Tokyo, 7-3-1 Hongo, Bunkyo-ku, Tokyo 113-0033, Japan

³Institute of Physics, University of Tokyo, Komaba, Meguro-ku, Tokyo 153-8902, Japan

⁴Institute of Nuclear Research of the Hungarian Academy of Sciences, H-4001 Debrecen, Hungary

⁵KFKI Research Institute for Particle and Nuclear Physics, H-1525 Budapest, Hungary

⁶RI Beam Science Laboratory, RIKEN, Wako, Saitama 351-0198, Japan

(Received 19 May 2003; published 18 September 2003)

A radio frequency quadrupole decelerator and achromatic momentum analyzer were used to decelerate antiprotons and produce $\bar{p}^4\text{He}^+$ and $\bar{p}^3\text{He}^+$ atoms in ultra-low-density targets, where collision-induced shifts of the atomic transition frequencies were negligible. The frequencies at near-vacuo conditions were measured by laser spectroscopy to fractional precisions of $(6\text{--}19) \times 10^{-8}$. By comparing these with QED calculations and the antiproton cyclotron frequency, we set a new limit of 1×10^{-8} on possible differences between the antiproton and proton charges and masses.

DOI: 10.1103/PhysRevLett.91.123401

PACS numbers: 36.10.-k, 14.20.Dh, 32.70.Jz

Recently, we measured some transition frequencies in antiprotonic ^4He atoms [1] ($\bar{p}^4\text{He}^+ \equiv e^- - \bar{p} - ^4\text{He}^{2+}$) to sub-ppm precision [2] at the Antiproton Decelerator (AD) of CERN. By comparing these with three-body QED calculations and using the measured value of the antiproton cyclotron frequency [3], a 60-ppb limit was obtained for the possible differences $\delta_{\bar{p}}$ between the antiproton and proton charges and masses. Any such difference, however small, would imply CPT violation, i.e., that physical laws are not perfectly invariant under a combined transformation of charge conjugation, parity, and time reversal [4]. The precision of the experiment [2] was limited by the high density of the cryogenic helium targets (atomic density $\rho \sim 10^{21} \text{ cm}^{-3}$, corresponding to pressures $p = 10\text{--}200$ bars at room temperature) used to stop the 5.3-MeV antiproton beam and produce these atoms. The $\bar{p}^4\text{He}^+$ underwent many collisions with helium atoms, resulting in large shifts [1,2,5] in the transition frequencies. We here report on new laser spectroscopy measurements at ultralow target densities of $\rho \sim 10^{17} \text{ cm}^{-3}$, some 10^4 times lower than those previously used. These experiments were made possible by a radio frequency quadrupole decelerator (RFQD, Fig. 1) [6], which decelerated the 5.3-MeV antiprotons used previously [2] to energies $E = 10\text{--}120$ keV. The collisional shifts thus became negligible ($|\Delta\nu| \leq 1$ MHz) compared to the natural widths of the transitions, so that the observed frequencies were effectively *in vacuo*. We also extended our high-precision studies to the isotope $\bar{p}^3\text{He}^+$, and to transitions which could not be observed at high densities, thus increasing the number of measured frequencies with small natural widths ($\Gamma < 50$ MHz) from 4 [2] to 13.

In these experiments, laser pulses induced antiproton transitions from metastable $\bar{p}\text{He}^+$ states (Fig. 2) with

large principal ($n \sim 38$) and angular momentum ($\ell \sim n$) quantum numbers, to states with short Auger lifetimes [1]. The two-body $\bar{p}\text{He}^{2+}$ ions formed after Auger emission suffered collisional Stark effects, which caused the rapid annihilation of the antiproton in the helium nucleus. The resulting spike in the rate of annihilations signaled the transition frequency. In previous experiments made at higher densities, collisions produced large frequency shifts ($|\Delta\nu| = 0.5\text{--}5.0$ GHz) which were of the order of $10^{-6}\text{--}10^{-5}$ of the measured transition frequencies ν . The frequencies $\nu_{\rho=0}$ for an isolated atom therefore had to be inferred by measuring transitions at several target densities and assuming a linear extrapolation to $\rho = 0$. The justification for this, however, was unclear due to the absence of data below $\rho \leq 3 \times 10^{20} \text{ cm}^{-3}$. In fact, the extrapolated value $\nu_{\rho=0}$ for the transition with the largest density shift [$(n, \ell) = (39, 35) \rightarrow (38, 34)$ at wavelength $\lambda = 597.3$ nm] disagreed with theoretical values by

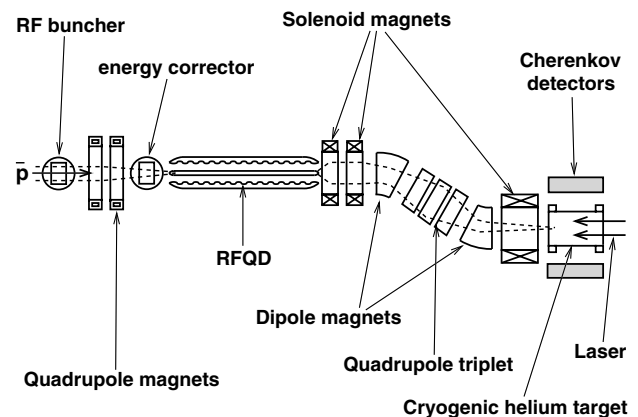


FIG. 1. Experimental layout. Dashed lines indicate trajectories of the antiproton beam. Drawing not to scale.

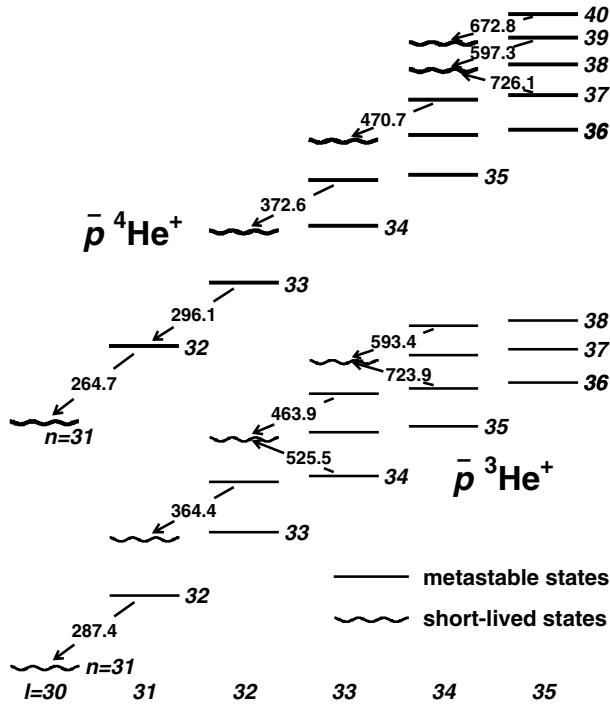


FIG. 2. Energy level diagrams of $\bar{p}^4\text{He}^+$ and $\bar{p}^3\text{He}^+$. Wavelengths of studied transitions are indicated in nanometers.

$(5-7) \times 10^{-7}$ [2]. Moreover, some transitions could not be observed; it was assumed that collisions destroy the antiprotonic populations in the associated states [2,7].

In the present experiment (Fig. 1), the AD produced a 100-ns-long pulsed beam containing 3×10^7 antiprotons at a repetition rate $f = 0.01$ Hz. A radio frequency bunching cavity shaped the pulse into a train of 20 micro-pulses, each 0.3 ns long with a separation $\Delta t = 5$ ns. These entered the RFQD, which consisted of a 3.5-m-long, four-rod electrode structure producing an average decelerating field $E \sim 2$ MV/m at frequency $f = 202.5$ MHz. Some $\sim 30\%$ of the antiprotons were emitted with energy $E = 65$ keV, energy spread $\Delta E \sim 10$ keV, and angular divergence $\theta = 30^\circ$; the remaining 70% emerged with little or no deceleration. The output energy could be varied between $E = 10$ and 120 keV by biasing the electrodes of the RFQD with a dc potential. An energy-correcting cavity at the input of the RFQD was used to compensate for the changes in the energy of the incident beam resulting from this biasing and variations in the energy of the antiprotons extracted from the AD. The decelerated antiprotons were diverted by an achromatic momentum analyzer connected to the output of the RFQD and focused into a 10-mm-diam spot at the entrance of the experimental target; this diversion eliminated the large background that the undecelerated antiprotons would have otherwise produced. The analyzer consisted of two dipole magnets which bent the beam twice at an angle $\theta = 20^\circ$, three 1-T solenoids which focused it, and three quadrupole magnets which transferred the focal plane at the RFQD exit to the position

of the target. Iron shields prevented magnetic fields from entering the target. The spatial profiles of antiproton pulses along the beam line were measured non-destructively by microwire secondary electron emission detectors.

The target was a 150-mm-diam, 300-mm-long cylindrical chamber filled with ^4He (purity 99.9999%) or ^3He (99.997%) gas, at pressures $p = 0.7-2$ mb and temperatures $T = 12-30$ K. The antiprotons entered through a 0.8- μm -thick polyethylene window mounted on one end of the chamber. Differential pumping removed the helium permeating through the thin window, thus maintaining a vacuum better than $p = 10^{-8}$ mb in the RFQD. The stopped antiprotons formed $\bar{p}\text{He}^+$ atoms filling the entire volume of the chamber, and these were irradiated by a 50-mm-diam laser beam entering through a fused silica window. Charged pions emerging from the annihilations produced Cherenkov light in acrylic plates. By detecting this light envelope using a photomultiplier [8], delayed annihilation time spectra (the distribution of the number of antiproton annihilations, as a function of time elapsed since $\bar{p}\text{He}^+$ formation) were observed.

A Nd:YAG-pumped dye laser produced 4–6-ns-long laser pulses with wavelengths $\lambda = 264-726$ nm and power densities $P = 0.1-3$ mJ/cm 2 . Annihilation spikes could be induced on the delayed annihilation time spectrum at any time $t = 0.3-15$ μs after formation [Fig. 3(a)]. The wavelength of each laser pulse was measured by a Fizeau wavelength meter and confocal etalon, and laser pulses with bandwidths exceeding ~ 0.6 GHz (typically half of them) were rejected. During the 100-s intervals between antiproton arrivals, the wavelengths were calibrated against iodine [9] and tellurium [10] lines measured by absorption spectroscopy, or neon [11] and argon [12] lines measured by optogalvanic spectroscopy.

At the ultralow target densities used here, $\bar{p}^4\text{He}^+$ [Fig. 3(a)] and $\bar{p}^3\text{He}^+$ had average lifetimes greater than $\tau_{\text{avg}} = 5$ μs and 4 μs , respectively, which are 1–2 μs longer than the values measured previously [1,7]. The $\bar{p}^4\text{He}^+$ transition $(32, 31) \rightarrow (31, 30)$ at 264.7 nm could not be detected in previous experiments [2], because the resonant parent state was found to have a

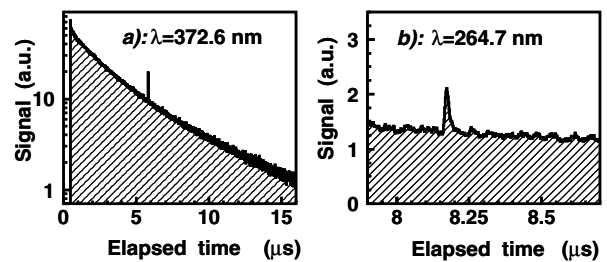


FIG. 3. Delayed annihilation time spectra of $\bar{p}^4\text{He}^+$ measured at ultralow densities $\rho \sim 5 \times 10^{17}$ cm $^{-3}$, with laser-induced annihilation spikes of the transitions $(35, 33) \rightarrow (34, 32)$ (a) and $(32, 31) \rightarrow (31, 30)$ (b). The latter transition could not be observed at higher densities.

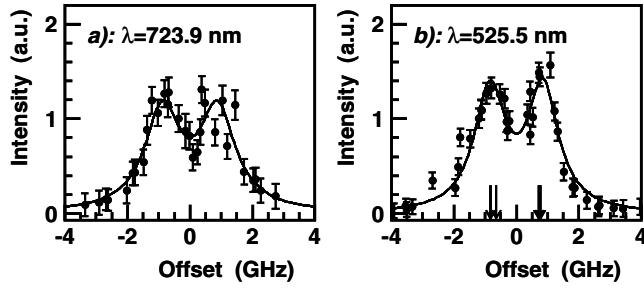


FIG. 4. Frequency profiles of $\bar{p}^3\text{He}^+$ transitions $(36, 34) \rightarrow (37, 33)$ (a) and $(34, 33) \rightarrow (35, 32)$ (b). Arrows denote theoretical positions of the substructure due to spin interactions; see text.

lifetime [$\tau_{(32,31)} = (8 \pm 1)$ ns] 2 orders of magnitude shorter than the theoretically expected value. Assuming that this discrepancy was caused by high-frequency collisions destroying the population in $(32, 31)$ [7], we expected that the state would recover its metastability at the low ($\rho \sim 5 \times 10^{17}$ cm $^{-3}$) densities of the present experiment, thus allowing us to detect the transition. Indeed, it was observed [Fig. 3(b)]. On the other hand, the adjacent transition $(33, 32) \rightarrow (32, 31)$ at 296.1 nm which was detected at higher densities [2] could no longer be observed as both parent and daughter states became long-lived, and the present detection method requires at least one of these to proceed rapidly to antiproton annihilation.

In Fig. 4(a), the resonance profile of the $\bar{p}^3\text{He}^+$ transition $(36, 34) \rightarrow (37, 33)$ at 723.9 nm is shown. The two-peak structure is the hyperfine splitting arising from the interaction between the orbital angular momentum of the antiproton and the electronic spin. The measured spacing $\Delta_{\text{HFS}} = 1.8 \pm 0.1$ GHz between the peaks agreed with theoretical calculations [13]. In Fig. 4(b), the profile of

the transition $(34, 33) \rightarrow (35, 32)$ at 525.5 nm is shown, with a hyperfine splitting $\Delta_{\text{HFS}} = 1.6 \pm 0.1$ GHz. Because of the spin interactions between the electron, antiproton, and ^3He nucleus, the profile is theoretically expected to be a superposition of eight partially overlapping peaks, the calculated positions of which are shown by arrows. The uneven spacings among the peaks causes a slight asymmetry in the profile as indeed seen in the figure. Possible errors in the determination of the resonance centroid due to this asymmetry were minimized by fitting the profile with four Voigt functions (solid lines), superimposed on each other and separated by the theoretical splittings. The resonances were 1–3 GHz wide, including contributions from the hyperfine structure, Doppler broadening, and laser linewidth. The experimental accuracy was limited by statistical and systematic fluctuations in the signal intensities which varied between 20 and 200 MHz depending on the transition and the 20–50-MHz accuracy of the laser frequency calibration.

The transition frequencies ν_{exp} in isolated $\bar{p}\text{He}^+$ atoms were thus directly measured (Table I). An exception was the $\bar{p}^4\text{He}^+$ transition $(33, 32) \rightarrow (32, 31)$ at 296.1 nm, which could not be observed as described above; we instead show data measured at higher densities [2]. The lower-lying $\bar{p}^3\text{He}^+$ transitions $(34, 33) \rightarrow (35, 32)$ at 525.5 nm, $(34, 32) \rightarrow (33, 31)$ at 364.4 nm, and $(32, 31) \rightarrow (31, 30)$ at 287.4 nm had very small frequency shifts [5], and so data measured at both ultralow and higher densities between $\rho = 10^{17}$ and 10^{21} cm $^{-3}$ were used to derive the final result. Experimental precisions of $(6\text{--}19) \times 10^{-8}$ were obtained, the highest being for the $\bar{p}^4\text{He}^+$ transition $(35, 33) \rightarrow (34, 32)$ at 372.6 nm. In Fig. 5, the frequencies are compared with the results ν_{th} of theoretical calculations [13–17], which include QED

TABLE I. Experimental and theoretical transition frequencies of isolated $\bar{p}\text{He}^+$ atoms. Values for f (see text) and the fractional difference $\delta_{\bar{p}}$ between the proton and antiproton charges and masses estimated from each transition are shown.

Transition ($n, \ell \rightarrow n', \ell'$)	Wavelength (nm) Expt.	Transition frequency (GHz)			f Kino [16]	$\delta_{\bar{p}}$ (parts per 10^9)
		Expt.	Korobov [17]	Kino [13]		
$\bar{p}^4\text{He}^+$ transitions						
$(40, 35) \rightarrow (39, 34)$	672.770 76(10)	445 608.63(7)	445 608.57	445 608.583	3.11	−40(50)
$(39, 35) \rightarrow (38, 34)$	597.257 04(5)	501 948.80(4)	501 948.765	501 948.769	4.45	−15(20)
$(37, 35) \rightarrow (38, 34)$	726.091 69(5)	412 885.13(3)	412 885.129	412 885.151	6.05	4(10)
$(37, 34) \rightarrow (36, 33)$	470.721 77(9)	636 878.24(12)	636 878.159	636 878.109	2.83	−60(70)
$(35, 33) \rightarrow (34, 32)$	372.582 83(2)	804 633.05(5)	804 633.053	804 633.020	2.54	−6(20)
$(33, 32) \rightarrow (32, 31)$	296.107 27(5)	1012 445.45(17)	1012 445.630	1012 445.635	2.45	70(70)
$(32, 31) \rightarrow (31, 30)$	264.691 88(5)	1 132 609.2(2)	1 132 609.218	1 132 609.186	2.38	1(80)
$\bar{p}^3\text{He}^+$ transitions						
$(38, 34) \rightarrow (37, 33)$	593.387 24(8)	505 222.28(7)	505 222.293	505 222.215	3.06	−17(40)
$(36, 34) \rightarrow (37, 33)$	723.878 50(8)	414 147.48(5)	414 147.518	414 147.479	4.05	16(30)
$(36, 33) \rightarrow (35, 32)$	463.945 45(8)	646 180.40(11)	646 180.434	646 180.331	2.85	−9(60)
$(34, 33) \rightarrow (35, 32)$	525.509 50(9)	570 479.61(10)	570 479.583	570 479.508	3.63	−30(40)
$(34, 32) \rightarrow (33, 31)$	364.352 35(3)	822 809.18(7)	822 809.178	822 809.124	2.64	−13(30)
$(32, 31) \rightarrow (31, 30)$	287.397 41(2)	1 043 128.60(8)	1 043 128.620	1 043 128.557	2.45	−4(30)

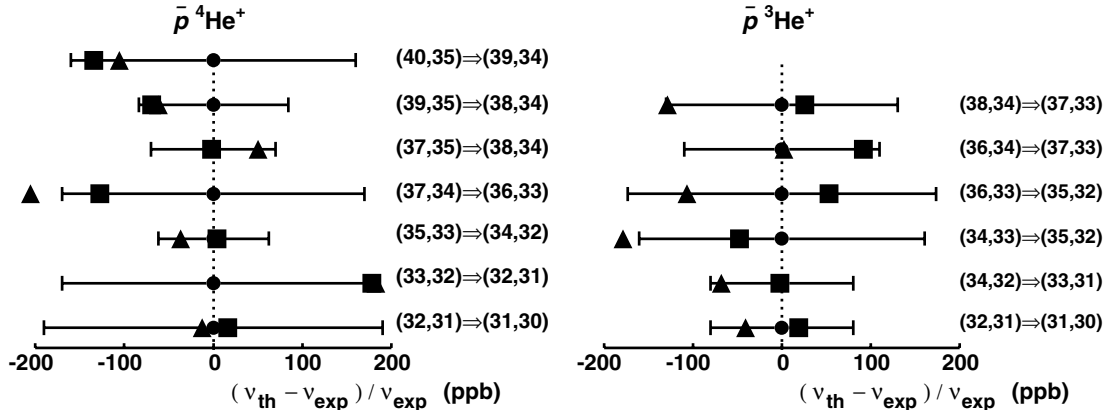


FIG. 5. Comparisons between experimental ν_{exp} (filled circles with errors) and theoretical ν_{th} (squares [17] and triangles [13]) transition frequencies of antiprotonic helium.

and finite nuclear-size effects. These claim an accuracy of 10^{-8} – 10^{-7} , limited by uncertainties in the three-body wave functions of states with large ($\Gamma > 10$ MHz) Auger widths; by using the complex coordinate rotation method [16,17], the precision has been improved compared to previous values [15] tabulated in Ref. [2]. In previous experiments [2], a theory-experiment difference of $|(\nu_{\text{th}} - \nu_{\text{exp}})/\nu_{\text{exp}}| \sim (5-7) \times 10^{-7}$ was observed in the $\bar{p}^4\text{He}^+$ transition $(39, 35) \rightarrow (38, 34)$ at 597.3 nm; as a result of these experimental and theoretical improvements, the difference has now been reduced to $< 8 \times 10^{-8}$.

By comparing the experimental and theoretical frequencies, a new upper limit $\delta_{\bar{p}}$ was set on the possible difference between the antiprotonic charge ($Q_{\bar{p}}$) and mass ($M_{\bar{p}}$) and those for the proton (Q_p, M_p). Following the method described in Refs. [1,2,18], we used the transition frequencies (which have a scale of the antiprotonic Rydberg constant $R_{\bar{p}} \propto M_{\bar{p}} Q_{\bar{p}}^2$) and the cyclotron frequency ($\omega_{\bar{p}} \propto Q_{\bar{p}} B / M_{\bar{p}}$) measured in Penning traps [3]. The limit $\delta_{\bar{p}}$ was deduced from the equation

$$\delta_{\bar{p}} = \frac{Q_p + Q_{\bar{p}}}{Q_p} \sim \frac{M_p - M_{\bar{p}}}{M_p} = \frac{1}{f} \frac{\nu_{\text{th}} - \nu_{\text{exp}}}{\nu_{\text{exp}}},$$

where ν_{th} is, for a given measured frequency ν_{exp} , the average of the two sets of theoretical values shown in Table I. Values for f were estimated [16] by changing the values of the antiproton charge and mass by 1 ppm under the constraint on $\omega_{\bar{p}}$ of 9×10^{-11} [3], and noting the change (2.5–6.1 ppm) in the calculated value ν_{th} . The $\bar{p}^4\text{He}^+$ transition $(37, 35) \rightarrow (38, 34)$ at 726.1 nm yielded an especially strong constraint on $\delta_{\bar{p}}$ of $(4 \pm 10) \times 10^{-9}$. By averaging over all 13 transitions, we obtained a mean value [$\delta_{\bar{p}} = (-3 \pm 7) \times 10^{-9}$] which was consistent with zero. From this we deduced that the antiproton charge and mass are in agreement with the proton's to a precision of 1×10^{-8} at a confidence level of 90%. Further progress requires improvements in both the experimental precision and QED calculations of $\bar{p}\text{He}^+$, which now have similar errors.

The RFQD was developed in collaboration with the CERN PS division and tested using the tandem accelerator at the University of Aarhus. We thank D. Bakalov, Y. Bylinsky, Y. Kino, H. Klette, V. I. Korobov, and A. M. Lombardi. This work was supported by the Grant-in-Aid for Creative Basic Research (10NP0101) of Monbukagakusho of Japan, and the Hungarian Scientific Research Fund (OTKA T033079 and TeT-Jap-4/00).

-
- [1] T. Yamazaki *et al.*, Phys. Rep. **366**, 183 (2002).
 - [2] M. Hori *et al.*, Phys. Rev. Lett. **87**, 093401 (2001).
 - [3] G. Gabrielse *et al.*, Phys. Rev. Lett. **82**, 3198 (1999).
 - [4] *Proceedings of the Second Meeting on CPT and Lorentz Symmetry, Bloomington, 2001*, edited by V. A. Kostelcký (World Scientific, Singapore, 2002).
 - [5] D. Bakalov *et al.*, Phys. Rev. Lett. **84**, 2350 (2000).
 - [6] A. M. Lombardi, W. Pirkel, and Y. Bylinsky, in *Proceedings of the 2001 Particle Accelerator Conference, Chicago, 2001* (IEEE, Piscataway, NJ, 2001), pp. 585–587.
 - [7] M. Hori *et al.*, Phys. Rev. A **57**, 1698 (1998); **58**, 1612(E) (1998).
 - [8] M. Hori *et al.*, Nucl. Instrum. Methods Phys. Res., Sect. A **496**, 102 (2003).
 - [9] B. Bodermann, H. Knöckel, and E. Tiemann, Eur. Phys. J. D **19**, 31 (2002), and references therein.
 - [10] J. Cariou and P. Luc, *Atlas du Spectre d'Absorption de la Molécule de Tellure* (CNRS II, France, 1980).
 - [11] E. S. Chang *et al.*, Phys. Scr. **49**, 26 (1994).
 - [12] W. Whaling *et al.*, J. Res. Natl. Inst. Stand. Technol. **107**, 149 (2002).
 - [13] Y. Kino *et al.*, in Proceedings of the International Conference on Low Energy Antiproton Physics, Yokohama, 2003 (unpublished).
 - [14] V. I. Korobov, Phys. Rev. A **54**, R1749 (1996).
 - [15] V. I. Korobov and D. D. Bakalov, Phys. Rev. Lett. **79**, 3379 (1997).
 - [16] Y. Kino *et al.*, Hyperfine Interact. **138**, 179 (2001).
 - [17] V. I. Korobov, Phys. Rev. A **67**, 062501 (2003).
 - [18] R. J. Hughes and B. I. Deutch, Phys. Rev. Lett. **69**, 578 (1992).